Journal of Power Sources 190 (2009) 341–345

Contents lists available at ScienceDirect

Journal of Power Sources

journal homepage: www.elsevier.com/locate/jpowsour

Short communication

Preparation of LSM–YSZ composite powder for anode of solid oxide electrolysis cell and its activation mechanism

Mingde Liang[a,b], Bo Yu[b,*], Mingfen Wen[b], Jing Chen[b], Jingming Xu[b], Yuchun Zhai[a]

[a] School of Materials and Metallurgy, Northeastern University, Shenyang 110004, PR China
[b] Institute of Nuclear and New Energy Technology, Tsinghua University, Beijing 102201, PR China

ARTICLE INFO

Article history:
Received 4 December 2008
Received in revised form 27 December 2008
Accepted 30 December 2008
Available online 14 January 2009

Keywords:
Hydrogen production
High-temperature steam electrolysis
Solid oxide electrolysis cells
Composite powder
Mechanism

ABSTRACT

Sr-doped $LaMnO_3$ and Yttria stabilized zirconia (LSM–YSZ) composite powder is synthesized by the preparation of LSM on submicron-sized YSZ particles using an in-situ glycin–nitrate combustion method for solid oxide electrolysis cells (SOEC) in this paper. LSM–YSZ composite powder and the relevant LSM powder are characterized by XRD and FESEM. The results show that LSM–YSZ is net-porous composite powder while YSZ and LSM do not react with each other during synthesis process. The electrochemical test of the single button cells indicates that the in-situ LSM–YSZ powder shows better electrolysis performance and lower discharging capability than traditionally direct mixture LSM and YSZ oxygen electrode. When operating in SOEC mode with constant current electrolysis at a current density of 0.33 A cm^{-2} and 900 °C, the electrolytic voltage decreases from 1.21 V to 1.02 V, which indicates that LSM–YSZ electrode has an activation process at the initial testing stage. A mechanism which involves the incorporation of SrO segregated on the surface into the LSM lattice and the generation of oxygen vacancies in the LSM electrode is proposed for the activation process with O^{2-} oxidation on LSM electrodes.

1. Introduction

Currently energy is developing to low- and non-carbon energy sources due to the global warming problem. Hydrogen has been widely identified as a potential alternative fuel as well as an energy carrier for the future energy supply [1,2]. High-temperature steam electrolysis (HTSE), which utilizes the heat and electrical power of renewable energy or advanced nuclear reactor as the energy sources of solid oxide electrolysis cells (SOEC) with high efficiency, provides a very promising way for the large-scale hydrogen production in the future [3–5].

The hydrogen production efficiency of HTSE increases with the increasing temperature [6]. Considering coupled with the high-temperature gas-cooled reactor (HTGR), the suitable operating temperature is in the range of 700–1000 °C [7]. As the high-temperature electrolysis is essentially a reverse process of solid oxide fuel cells (SOFC) in principle, the approach of SOEC was based on the existing materials and fabrication technology developed for high-temperature SOFC [8]. Strontium-doped lanthanum manganite (LSM) has been utilized as the most common oxygen electrode materials of SOEC due to its good electronic conductivity, catalytic properties for oxygen ion oxidation and mechanical/chemical compatibility with yttria-stabilized zirconia (YSZ) electrolyte [9]. However, the poor ionic conductivity limits the improvement of LSM performances owing that the reaction only occurs in a small area between electrolyte and oxygen electrode. The alternative way is to fabricate LSM with YSZ to form composite electrode which can extend the electrochemical active area to a certain depth of oxygen electrode. Nowadays, LSM–YSZ composite electrodes are mainly prepared by mixing as-prepared LSM and YSZ powders directly [10,11]; it is an effective way, however, the slurry containing two different particles is unstable which causes the non-uniform distribution between the LSM and YSZ grains, therefore, the LSM/YSZ/gas three phase boundaries (TPBs) decrease. Moreover, according to the reaction of oxygen electrodes, the opposite polarization direction demands that oxygen electrodes should have more adsorptive-desorption of oxygen in SOFC while have higher oxygen evolution property in SOEC mode. This may result in the traditionally mixed LSM and YSZ oxygen electrode which is suitable for SOFC application are not the best choice for SOEC.

It is known that freshly prepared (without polarization treatment) LSM electrodes can be significantly activated with the application of cathodic polarization/current passage with respect to the SOFC mode [12]. When applied an anodic polarization/current to the cathodically polarized LSM electrode, the electrochemical activity of oxygen reduces. Much work has been done on the activation and deactivation mechanism, and generally interpreted based on the generation and consumption of oxygen vacancies under cathodic and anodic polarization potential, respectively [13–18].

* Corresponding author. Tel.: +86 10 80194039; fax: +86 10 62771740.
E-mail address: cassy_yu@mail.tsinghua.edu.cn (B. Yu).

0378-7753/$ – see front matter © 2009 Elsevier B.V. All rights reserved.
doi:10.1016/j.jpowsour.2008.12.132

However, we found that the anodic current passage treatment also could significantly enhance the electrochemical activity of the freshly prepared LSM–YSZ electrodes in SOEC mode. To the best of the author's knowledge, there are few publications on the mechanism of the anodic polarization/current passage effect on freshly prepared LSM–YSZ electrodes.

Thus, the aim of this paper is to prepare high homogeneity and high performance LSM–YSZ composite powder through synthesized LSM on submicron-sized YSZ particles using an in-situ glycin–nitrate combustion method for SOEC. Based on the electrochemical test results, a mechanism for the activation process on LSM–YSZ electrode in SOEC mode is also proposed.

2. Experimental

2.1. Preparation and characterization of LSM–YSZ composite powder

LSM–YSZ composite powder was synthesized by an in-situ glycin–nitrate combustion method. Lanthanum nitrate, strontium nitrate, manganous nitrate and YSZ powder (TZ-8Y, Tosoh Corporation, Japan) were used as raw materials in this method. The nitrates in the proportion of $(La_{0.75}Sr_{0.25})_{0.95}MnO_3$ were dissolved in deionized water. Then glycin and YSZ powder were added to the nitrate aqueous solution and ultrasonically separated for 15 min to form emulsion. The molar ratio of metal ions and glycin was 9:5. The weight ratio of YSZ to theoretically generative LSM was controlled at 4:6. After adjusted pH value of the solution to 7 with ammonia, the mixture was stirred at 80 °C for 0.5 h and then heated in a porcelain dish. As the evaporation proceeded, the emulsion became viscous, and changed to a foamy black sponge. Finally it was self ignited from the bottom and the whole combustion process finished instantaneously. The as-burned loose powder was then treated at 1000 °C in the air for 2 h and LSM–YSZ composite powder was obtained.

For comparison, pure LSM powder was synthesized under the same conditions. Then the LSM powder was mixed with YSZ thoroughly in a weight ratio of 6:4 by ball milling. The cells prepared by situ-precipitation LSM–YSZ composite powder and ball milling LSM–YSZ powder were named as cell-A and cell-B for convenient discussion in this paper, respectively.

The crystalline phase of the synthesized powders were analyzed by an X-ray diffraction (XRD, D8 Advance, BRUKER Corporation, Germany), using Cu Kα radiation (λ = 0.15406 nm). The morphology of the LSM–YSZ and LSM powders were observed by a field emission scanning electronic microscope (FESEM, QUANTA 200F, FEI Corporation, USA).

2.2. Fabrication and electrochemical test of the single electrolysis cells

NiO-YSZ hydrogen electrode was prepared by dry pressing process. To form sufficient porosity, starch was added as a pore former. NiO-YSZ composite powder and starch were fully mixed in a weight ratio of 5:1 by ball milling. The mixed powder was then pressed into a disc with 20 mm in diameter and 500 μm in thickness under a pressure of 250 MPa. Then the green discs were pre-sintered at 800 °C for 2 h.

The YSZ electrolyte and LSM–YSZ oxygen electrode were fabricated by screen-printing method. The printing ink was the combination of functional powder with the organic binder by ball milling for 2 h. The organic binder was prepared by dissolving 5 wt% ethylcellulose into 95 wt% terpineol. The weight ratio of functional powder to organic binder in electrolyte and oxygen electrode printing ink was 3:4 and 2:3, respectively. To obtain dense YSZ films, YSZ powder was ball-milled for 24 h with ethanol adding before prepared electrolyte printing ink. Then the electrolyte screen-printed on the NiO-YSZ electrode and sintered at 1400 °C for 4 h. LSM–YSZ oxygen electrode layer with an effective area of 0.9 cm^2 was deposited onto the sintered YSZ film subsequently and sintered at 1180 °C for 2 h in the air.

The cells were tested with a DC 4-probe technique at 900 °C. The feed gas to the hydrogen electrode was the mixture of H_2/H_2O and ambient air on the oxygen electrode side. IM6ex electrochemical workstation (Zahner IM6ex, Germany) was employed to measure the cell performance. Current–voltage (*I–V*) curves were tested by linear sweep voltammetry at a scanning rate of 10 mV s^{-1}. The durability of the cells was observed by means of constant current electrolysis with a current density of 0.33 A cm^{-2}. The spectra were recorded applying an AC voltage with amplitude of 10 mV in the frequency range from 100 kHz to 0.5 Hz under open-circuit conditions. The microstructure of the cell was examined using a FESEM.

3. Results and discussion

3.1. Powder characteristics

Fig. 1 is the X-ray diffraction patterns of LSM–YSZ and LSM powders calcined at 1000 °C for 2 h in the air. The results show that YSZ is cubic phase in sample (a) and LSM presents perovskite structure in sample (a) and (b). In the LSM–YSZ composite powder, there are no other diffraction peaks except YSZ and LSM X-ray diffraction patterns, which indicates that YSZ and LSM do not react with each other during synthesis process.

Fig. 2a and b is FESEM micrograph of LSM–YSZ and LSM powders calcined at 1000 °C for 2 h in the air, respectively. Both powders are porous while LSM powders agglomerate to form spongy structure as well as LSM–YSZ composite powder shows porous and net structure. YSZ powders are coated by LSM and functioned as the skeletons of the net structure.

3.2. Electrochemical performance of the cells

The FESEM micrographs of the cross-section views of hydrogen electrode supported single cell: (a) cell-A and (b) cell-B are shown in Fig. 3. Each single cell consists of three layers, porous Ni-YSZ hydrogen electrode (500 μm thick), dense YSZ electrolyte (12 μm thick), and porous LSM–YSZ oxygen electrode (50 μm thick). In Fig. 3a, the LSM–YSZ grain size is almost equivalent to the branch coarseness of the net LSM–YSZ composite powder in Fig. 2a. And the LSM grain size in the oxygen electrode of cell-B (Fig. 3b) is much smaller than

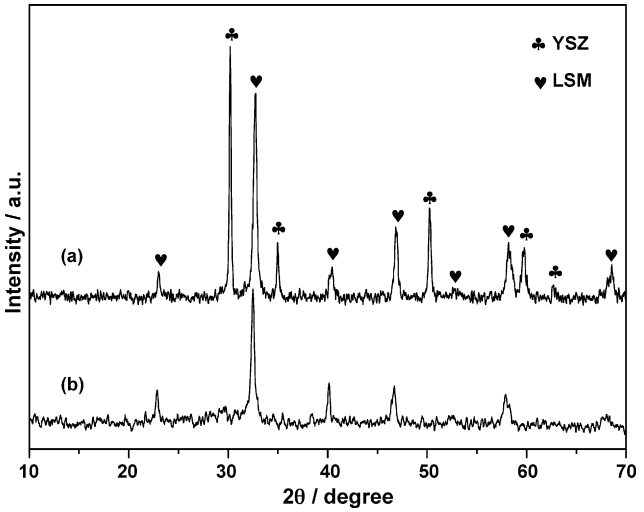

Fig. 1. XRD patterns of (a) LSM–YSZ composite powder and (b) LSM powder calcined at 1000 °C for 2 h.

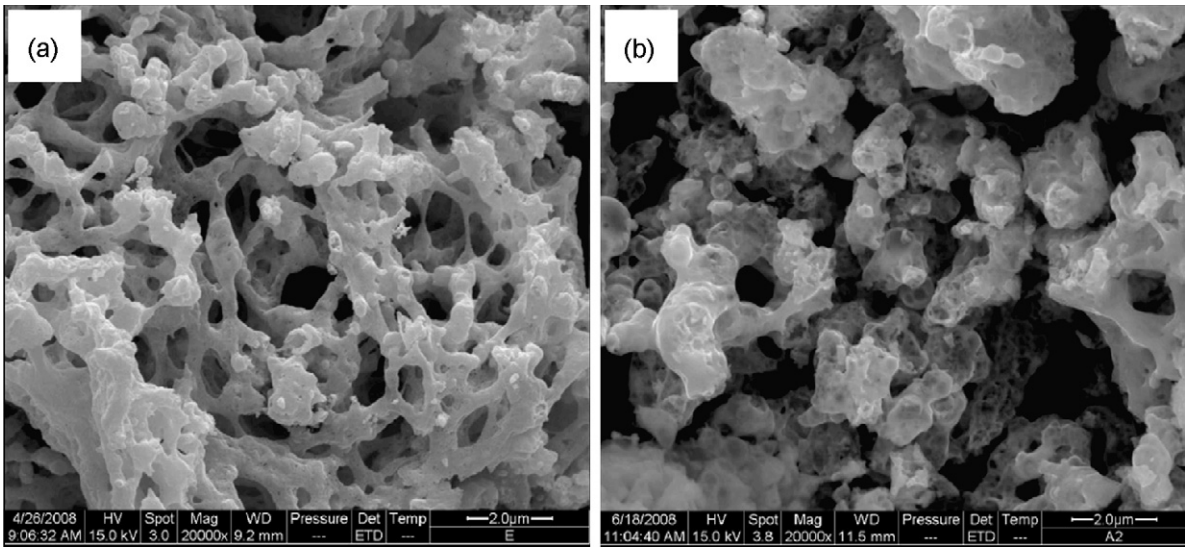

Fig. 2. FESEM micrographs of (a) LSM–YSZ composite powder and (b) LSM powder calcined at 1000 °C for 2 h.

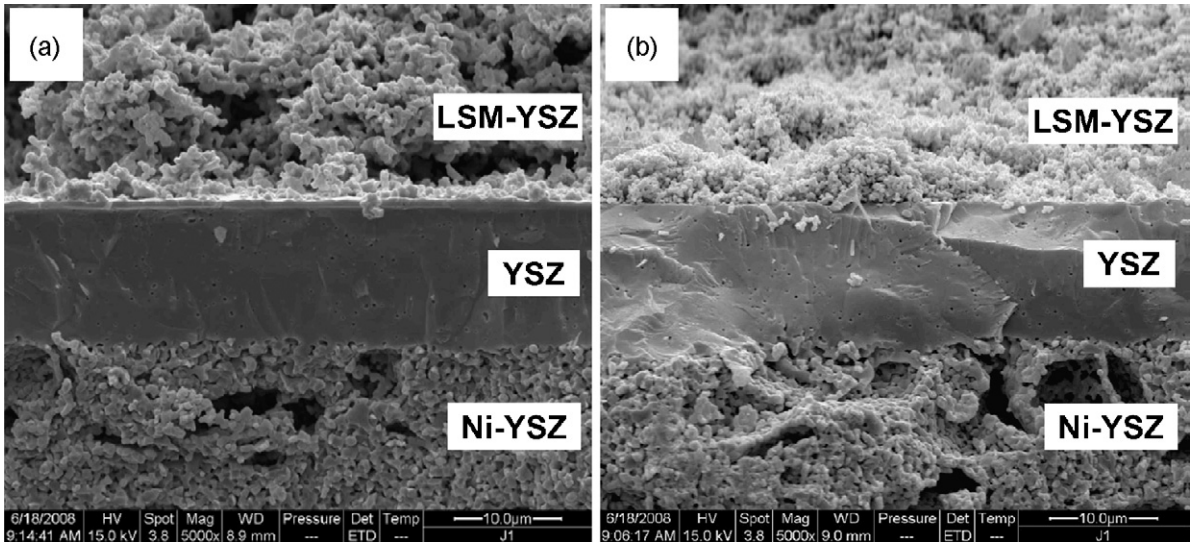

Fig. 3. FESEM micrographs of the post-test cell: (a) Cell-A and (b) Cell-B.

that in Fig. 2b. It indicates that LSM and YSZ are in close contact with LSM–YSZ composite powder which is harder to be cracked than spongy LSM powder in LSM–YSZ printing ink preparation process.

Fig. 4 shows the performances of single cells tested at 850 °C and 900 °C, the input stream of 60% H_2O + 40% H_2 to hydrogen electrode and the air to oxygen electrode, respectively. The hydrogen flow rate was set at 30 mL min^{-1}. Since the Ni-YSZ hydrogen electrode and YSZ electrolyte of cell-A and cell-B were similar, the only changeable parameter is the LSM–YSZ oxygen electrode. The open-circuit voltage (OCV) of cell-A and cell-B were 0.883 V and 0.886 V at 900 °C, respectively. Both were near the theoretical OCV value (0.888 V) calculated from Nernst formula, which suggested that the YSZ film was quite dense and that the fuel gas leakage through the YSZ film could be negligible. In the SOEC mode, the current densities of cell-A and cell-B were −0.520 A cm^{-2}, −0.431 A cm^{-2} at 900 °C and −0.333 A cm^{-2}, −0.231 A cm^{-2} at 850 °C at 1.50 V, respectively. In the SOFC mode, the current densities of cell-A and cell-B were 0.501 A cm^{-2}, 0.600 A cm^{-2} at 900 °C and 0.383 A cm^{-2}, 0.459 A cm^{-2} at 850 °C under 0.38 V discharging voltage, respectively. Compared with cell-B, cell-A had better electrolysis performance and lower discharging capability.

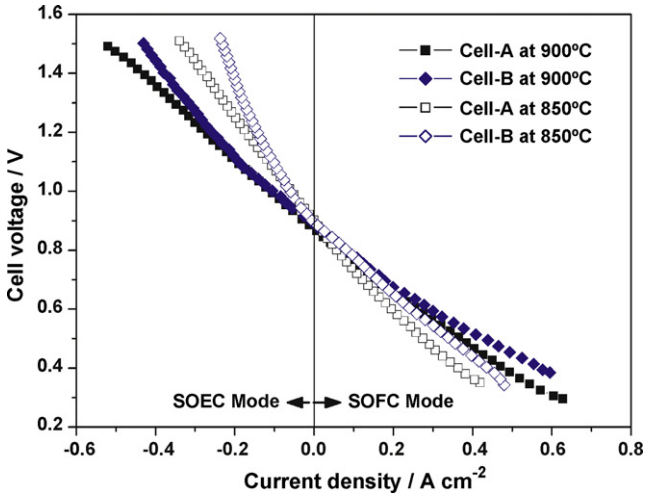

Fig. 4. Comparison of *I–V* curves recorded at 850 °C and 900 °C for the cell-A and cell-B. 60% H_2O + 40% H_2 and ambient air were used as inlet gas to the hydrogen electrode and oxygen electrode, respectively.

3.3. Mechanism of LSM–YSZ oxygen electrode in SOEC mode

It has been well known that the electrochemical activity of the freshly prepared LSM electrodes can be significantly improved with the application of cathodic polarization/current passage. Wang and Jiang [12] had studied the activation process for the O_2 reduction on LSM electrodes using Pt/YSZ/LSM cell and proposed a mechanism as follows:

$$V'_{La,LSM} + SrO + 3Mn^{\bullet}_{Mn,LSM} + e' \rightarrow Sr'_{La,LSM} + O^{X}_{O,LSM} + 3Mn^{X}_{Mn,LSM} \quad (1)$$

$$O^{X}_{O,LSM} + 2Mn^{\bullet}_{Mn,LSM} + V^{\bullet\bullet}_{O,YSZ} + 2e' \rightarrow V^{\bullet\bullet}_{O,LSM} + 2Mn^{X}_{Mn,LSM} + O^{X}_{O,YSZ} \quad (2)$$

$$O^{X}_{O,LSM} + 2Mn^{X}_{Mn,LSM} + V^{\bullet\bullet}_{O,YSZ} + 2e' \rightarrow V^{\bullet\bullet}_{O,LSM} + 2Mn'_{Mn,LSM} + O^{X}_{O,YSZ} \quad (3)$$

where $V'_{La,LSM}$ is the cation vacancy on LSM lattice sites; $Sr'_{La,LSM}$ represents a Sr ion introduced into a La lattice site in LSM; $Mn^{\bullet}_{Mn,LSM}$, $Mn^{X}_{Mn,LSM}$ and $Mn'_{Mn,LSM}$ are Mn^{4+}, Mn^{3+} and Mn^{2+} ions; $O^{X}_{O,LSM}$ and $O^{X}_{O,YSZ}$ are the O^{2-} ions in LSM and YSZ lattice sites; $V^{\bullet\bullet}_{O,LSM}$ and $V^{\bullet\bullet}_{O,YSZ}$ stand for oxygen vacancies, respectively. Under cathodic polarization potential, the segregated SrO on LSM surface is incorporated into the LSM lattice structure with the concomitant reduction of Mn ions, as illustrated by Eq. (1). Further cathodic polarization will lead to the generation and propagation of oxygen vacancies, as shown by Eqs. (2) and (3). The removal of the inhibiting SrO species and formation of oxygen vacancies may increase active sites on the LSM surface, enhancing the adsorption and diffusion of oxygen on the LSM surface. When applied an anodic current to prior cathodically polarized LSM electrode, the oxygen vacancies can be consumed by the recombination reactions, followed by the re-segregation of SrO onto the LSM surface with the concomitant generation of cation vacancies in the LSM lattice structure, that is the backward reactions of Eqs. (1), (2) and (3), respectively.

Although LSM–YSZ electrodes in SOEC mode were under anodic polarization potential, we found that the anodic current passage treatment also could significantly enhance the electrochemical activity of the freshly prepared LSM–YSZ electrodes, as shown in Fig. 5. Cell-A was tested at 900 °C by means of constant current electrolysis with a current density of 0.33 A cm^{-2}. The inlet gas to Ni-YSZ hydrogen electrode was 60% H_2O + 40% H_2 at a rate of 75 mL min^{-1} and oxygen electrode was in the air. At the initial testing stage, the electrolytic voltage decreased gradually from 1.21 V to 1.03 V, which is corresponding to the activation process of LSM–YSZ electrode. During the operation at 0.33 A cm^{-2} between 20 and 120 min, the electrolytic voltage was approximately stable at 1.02 V.

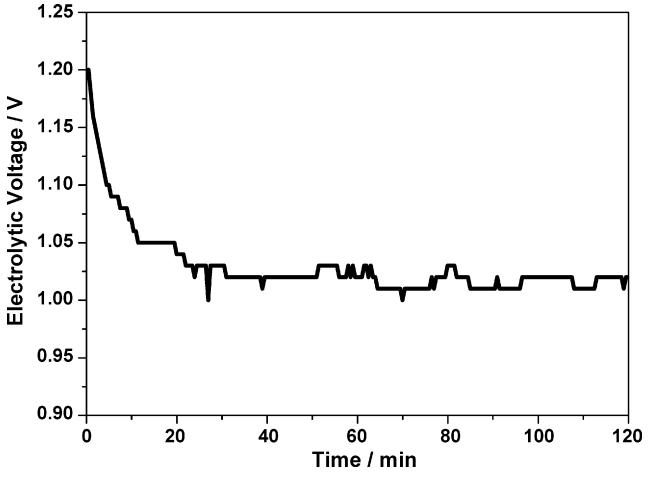

Fig. 5. Constant current electrolysis testing of cell-A with a current density of 0.33 A cm^{-2} at 900 °C. 60% H_2O + 40% H_2 and ambient air were used as inlet gas to the hydrogen electrode and oxygen electrode, respectively.

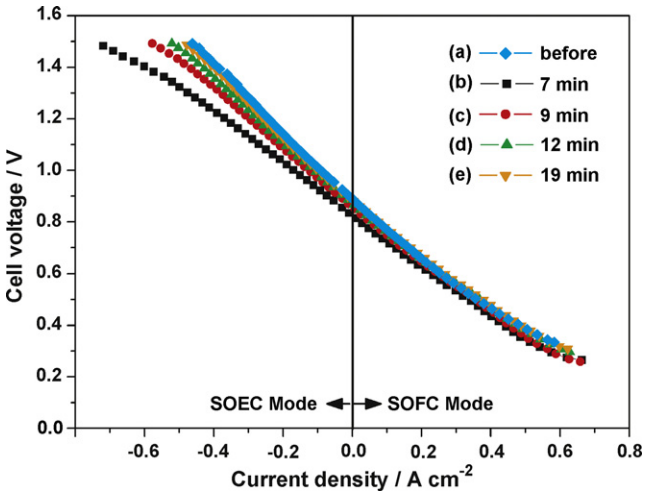

Fig. 6. *I–V* curves recorded for cell-A (a) before and (b), (c), (d), (e) after 120 min constant current electrolysis at 900 °C. 60% H_2O + 40% H_2 and ambient air were used as inlet gas to the hydrogen electrode and oxygen electrode, respectively.

When under open-circuit, there was a deactivation process occur on the anodically polarized LSM–YSZ electrodes. After constant current electrolysis for 120 min, cell-A's OCV was 0.680 V. And the value of OCV increased to 0.885 V after stopping constant current electrolysis for 19 min, which were almost equivalent to the OCV before constant current electrolysis. Fig. 6 shows *I–V* curves of cell-A recorded by linear sweep voltammetry at different times. After stopping the electrolysis current, the electrochemical performance decreased with the time in SOEC mode and almost kept invariant in SOFC mode. The impedance spectra of cell-A recorded before and after 120 min constant current electrolysis at 900 °C was shown in Fig. 7. The ohmic resistance increased from 0.32 Ω cm^2 to 0.40 Ω cm^2 and polarization resistance increased from 0.46 Ω cm^2 to 0.71 Ω cm^2 from 3 to 22 min. The impedance increasement of cell-A was consistent with the change of *I–V* curves in SOEC mode recorded after constant current electrolysis. Meanwhile, the 17th and 22nd minute impedances had almost the same ohmic resistance and high-frequency arc with impedance

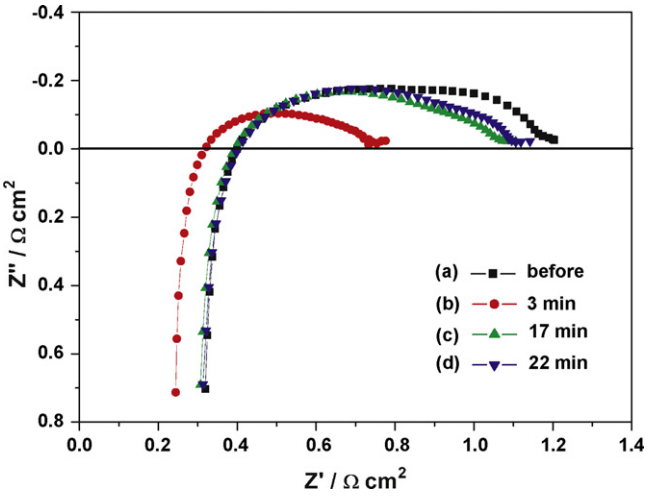

Fig. 7. Impedance spectra of cell-A recorded at different time: (a) before and (b), (c), (d) after 120 min constant current electrolysis at 900 °C.

recorded before constant current electrolysis, but obvious smaller low-frequency arc. As the atmosphere of hydrogen and oxygen electrodes was stable, the change of OCV and electrolysis performance was caused by oxygen electrode deactivation. Moreover, the value of OCV increased (0.885 − 0.680 = 0.205 V) after stopping constant current electrolysis were almost equal to that decreased one (1.21 − 1.03 = 0.18 V) in Fig. 5, which indicated that the activation and deactivation may be reversible in SOEC mode.

Through experimental results and analysis above we can find that the initial electrode interface resistance for the O^{2-} oxidation on the freshly prepared LSM–YSZ electrodes in SOEC mode can be significantly reduced with the application of anodic polarization, while the deactivation occur when stop the anodic current passage. Therefore, a model of LSM perovskite based on the above considerations and articles [12,16,19] is proposed for the activation/deactivation processes of LSM–YSZ electrodes under anodic polarization condition in SOEC mode.

At the beginning stage of electrolysis, O^{2-} oxidation reaction mainly occurs on the three phase boundaries consisted of LSM grains, YSZ grains and air as the low oxygen ion diffusion coefficient of LSM, as follows:

$$O^{X}_{O,YSZ} - 2e' \rightarrow V^{\bullet\bullet}_{O,YSZ} + \frac{1}{2}O_2 \quad (4)$$

Under anodic polarization potential, manganese ions at the LSM lattice and interstitial sites are reduced and segregated SrO on LSM surface is incorporated into the LSM lattice structure with the concomitant generation of oxygen vacancies in LSM because of the oxidation of O^{2-}, as follows:

$$2Mn^{\bullet}_{Mn,LSM} + O^{X}_{O,LSM} \rightarrow 2Mn^{X}_{Mn,LSM} + V^{\bullet\bullet}_{O,LSM} + \frac{1}{2}O_2 \quad (5)$$

$$V'_{La,LSM} + SrO + 2Mn^{\bullet}_{Mn,LSM} \rightarrow Sr'_{La,LSM} + 2Mn^{X}_{Mn,LSM} + V^{\bullet\bullet}_{O,LSM} + \frac{1}{2}O_2 \quad (6)$$

$$O^{X}_{O,YSZ} + V^{\bullet\bullet}_{O,LSM} + 2Mn^{X}_{Mn,LSM} - 2e' \rightarrow O^{X}_{O,LSM} + V^{\bullet\bullet}_{O,YSZ} + 2Mn^{\bullet}_{Mn,LSM} \quad (7)$$

The removal of the inhibiting SrO species may increase active sites on the LSM surface and the formation of oxygen vacancies in LSM (as illustrated by Eq. (6)) may enhance the transport and diffusion of oxygen ions in LSM–YSZ electrodes (as illustrated by Eq. (7)), resulting in higher electrolysis performance than the freshly prepared LSM–YSZ electrodes (Fig. 5).

When stop the anodic current, the oxygen vacancies can be consumed by the recombination reactions due to the reverse reactions of Eqs. (5) and (6) which are spontaneous process. SrO re-segregates onto the LSM surface with the concomitant generation of cation vacancies in the LSM lattice structure. The deactivation process to anodically polarized LSM–YSZ electrode could also occur for the cathodic current passage in SOFC mode. The decrease of oxygen vacancies and re-segregation of SrO lead to the increase of the ohmic resistance and polarization resistance (Fig. 7), respectively. Moreover, as the spontaneously proceed of reverse reactions of Eqs. (5) and (6) have directionality and need to consume oxygen potential, the OCV is less than theoretical value calculated from Nernst formula and the active sites on anodically polarized LSM was ineffective in SOFC mode, which was shown in Fig. 6.

4. Conclusions

LSM–YSZ composite powder was synthesized by the preparation of LSM on submicron-sized YSZ particles using glycin–nitrate combustion method for SOEC. XRD and FESEM analysis showed that YSZ and LSM did not react with each other during synthesis process and LSM–YSZ composite powder showed porous net structure. Single cells test indicated that the in-situ LSM–YSZ composite powder had better electrochemical performance than traditional LSM and YSZ mixture oxygen electrode. In SOEC mode, the anodic current passage treatment could enhance the electrochemical activity of the freshly prepared LSM–YSZ electrodes and a deactivation process occurred under the open-circuit or cathodic current passage on the anodically polarized LSM–YSZ electrodes. Based on the experiment results, a mechanism was proposed for the activation process for the O^{2-} oxidation on LSM–YSZ electrodes, which involved the incorporation of surface segregated SrO into the LSM lattice and generation of oxygen vacancies in the LSM–YSZ electrodes.

Acknowledgements

This work was supported by National Natural Science Foundation of China (No: 20803039). The authors would like to thank Dr. Wenqiang Zhang and Dr. Mingyi Liu for their help and assistance.

References

[1] J.S. Herring, J.E. O'Brien, C.M. Stoots, G.L. Hawkes, J.J. Hartvigsen, M. Shahnam, Int. J. Hydrogen Energy 32 (2007) 440–450.
[2] A. Brisse, J. Schefold, M. Zahid, Int. J. Hydrogen Energy 33 (2008) 5375–5382.
[3] B. Yu, W.Q. Zhang, J.M. Xu, J. Chen, Int. J. Hydrogen Energy 33 (2008) 6873–68772.
[4] A. Hauch, S.H. Jensen, S. Ramousse, M. Mogensen, J. Electrochem. Soc. 153 (2006) A1741–A1747.
[5] B. Yu, W.Q. Zhang, J. Chen, J.M. Xu, S.R. Wang, Sci. China. Ser. B 51 (2008) 289–304.
[6] M.Y. Liu, B. Yu, J.M. Xu, J. Chen, J. Power Sources 177 (2008) 493–499.
[7] S.H. Jensen, P.H. Larsen, M. Mogensen, Int. J. Hydrogen Energy 32 (2007) 3253–3257.
[8] M. Ni, M.K. Leung, D.Y. Leung, Int. J. Hydrogen Energy 33 (2008) 2337–2354.
[9] H.S. Song, W.H. Kim, S.H. Hyun, J. Moon, J. Kim, H.W. Lee, J. Power Sources 167 (2007) 258–264.
[10] J.H. Piao, K.N. Sun, N.Q. Zhang, S. Xu, J. Power Sources 175 (2008) 288–295.
[11] X.D. Ge, X.Q. Huang, Y.H. Zhang, Z. Lu, J.H. Xu, K.F. Chen, D.W. Dong, Z.G. Liu, J.P. Miao, W.H. Su, J. Power Sources 159 (2006) 1048–1050.
[12] W. Wang, S.P. Jiang, Solid State Ionics 177 (2006) 1361–1369.
[13] R.E. Cook, K.C. Goretta, J. Wolfenstine, P. Nash, J.L. Routbort, Acta Mater. 47 (1999) 2969–2980.
[14] J.S. Kim, S.I. Pyun, H.C. Shin, S.J.L. Kang, J. Electrochem. Soc. 155 (2008) B762–B769.
[15] T. Horita, K. Yamaji, N. Sakai, H. Yokokawa, T. Katob, J. Electrochem. Soc. 148 (2001) J25–J30.
[16] H.Y. Lee, W.S. Cho, S.M. Oh, H.-D. Wiemhöfer, W. Göpel, J. Electrochem. Soc. 142 (1995) 2659–2664.
[17] H. Xiaoa, T.L. Reitz, M.A. Rottmayer, J. Power Sources 183 (2008) 49–54.
[18] X.J. Chen, K.A. Khor, S.H. Chan, Solid State Ionics 167 (2004) 379–387.
[19] S.P. Jianga, J.G. Love, Solid State Ionics 138 (2001) 183–190.